Biophysical Reviews and Letters, Vol. 2, No. 2 (2007) 155–166

World Scientific
www.worldscientific.com

FLUCTUATIONS OF SINGLE CONFINED ACTIN FILAMENTS

SARAH KÖSTER*, HOLGER STARK† and THOMAS PFOHL‡,§

Max Planck Institute for Dynamics and Self-Organization
Bunsenstraße 10, 37073 Göttingen, Germany
**sarah.koester@ds.mpg.de*
†*holger.stark@ds.mpg.de*
‡*thomas.pfohl@ds.mpg.de*

JAN KIERFELD

Max Planck Institute of Colloids and Interfaces
Science Park Golm, 14424 Potsdam, Germany
jan.kierfeld@mpikg.mpg.de

Received 26 July 2006
Revised 13 November 2006

Thermal fluctuations of individual actin filaments confined in rectangular microchannels with dimensions similar to the mesh size of the cytoskeleton in eukaryotic cells are studied experimentally using fluorescence microscopy and theoretically by a combination of analytical methods and Monte Carlo simulations. Compared to freely fluctuating filaments, long filaments confined in narrow channels exhibit enhanced tangent correlations and a characteristic shape of their correlation function. The tangent correlation function is calculated analytically by approximating the confining geometry by a parabolic potential. This approximation is validated by Monte Carlo simulations. For the quantitative analysis of experimental data additional corrections for image analysis effects have to be included, for which we provide a modified analytical approximation formula which is corroborated by simulations. This allows us to obtain both the persistence length L_P describing the bending rigidity of the polymer and the deflection length λ characterizing confinement effects from fits to the experimental data. Our results confirm the scaling relation $\lambda \propto d^{2/3}$ between the deflection length and the channel width d.

Keywords: Actin; filaments; semiflexible polymers; confinement; single molecules.

1. Introduction

Actin is among the most abundant proteins in the eukaryotic cell. A dense network of actin filaments (F-actin) plays a key role in numerous crucial cellular processes such as cell motility, proliferation, and shape. Furthermore, it is one

§Corresponding author.

of the principal components of the cytoskeleton and, therefore, responsible for the mechanical stability of the cell. Thus, the mechanical and dynamic properties of actin and its supramolecular organization are important issues in cell biology.[1] In addition to its considerable importance in life science, actin also serves as one of the few experimentally accessible model systems for semiflexible polymers.[2,3] Globular actin (G-actin) monomers assemble into a two-stranded helical actin filament with a diameter of about 8 nm and a helical pitch of 37 nm. The contour length, L, of the filaments reaches up to 100 μm. Previous measurements on unconfined actin filaments revealed a persistence length, L_P, of 7.4–22 μm.[2–8] F-actin is thus intermediate between stiff biopolymers (e.g. microtubules, $L_P \sim 5.2$ mm) and flexible biopolymers (e.g. DNA, $L_P \sim 50$ nm). Since the contour length is within the range of optical resolution, fluorescently labeled actin filaments can be directly observed using optical microscopy. The experimental and theoretical understanding of the mechanical properties of the cytoskeleton is still incomplete.[9,10] Therefore, extensive efforts have been made to model the cellular mechanics using purified reconstituted *in vitro* systems. In recent years, several experimental studies on freely fluctuating actin filaments in dilute solutions have been performed, elucidating some of the mechanical and statistical properties of these biopolymers.[2–6,11,12] Considering the rather dense network of filamentous proteins within a eukaryotic cell (mesh size $\sim \mu$m), it is of substantial interest to regard the individual filament in an environment that resembles its native surrounding.[13,14] In addition, investigations of biopolymers in confining geometry are important for the fundamental understanding of the corresponding biological systems as well as for microfluidic applications on lab-on-a-chip platforms.[15–17]

In this letter, we present an analysis of thermal fluctuations of individual actin filaments confined in microchannels using a combination of experimental and theoretical methods. In the experiments, microchannels with dimensions of about the same order of magnitude as the mesh size of the cytoskeleton mimic the restraining network in the cell. Using fluorescence microscopy we directly visualize thermal fluctuations of individual actin filaments in the microchannels and show that the mechanical and dynamic properties of the semiflexible polymers are strongly dependent on the channel width, d. Using Monte Carlo simulations we show that tangent correlations of filaments can be quantitatively described using the worm-like chain (WLC) model and approximating the confining potential of the channel walls as a parabolic potential. The experimental tangent correlation data deviates from this result because of image analysis effects, and we identify the increased width of the filament image in fluorescence microscopy as the main effect. We provide a modified analytical approximation formula for tangent correlations with one additional fit parameter which captures this image analysis effect, and check the approximation formula using simulations. We use this new method to analyze the experimental data and to extract the persistence length L_P and the deflection length λ of the confined filaments.

2. Experimental Methods and Observations

Rhodamine labeled G-actin (Cytoskeleton, Denver, USA) was polymerized, stabilized using phalloidin, and diluted to a final monomer concentration of 70 nM. The detailed procedure is described elsewhere.[18] To avoid photobleaching and breakage of the filaments during observation, antifade solution was added just before performing the experiments.

The microchannels were fabricated using standard soft lithography techniques.[19,20] Briefly, SU-8 2 photo resist (Micro Resist Technology GmbH, Berlin, Germany) was spin coated onto a cleaned silicon wafer to a thickness of 0.9–1.4 μm. The coated wafers were then selectively exposed to UV light through a high resolution chrome mask and developed. The three dimensional structures (parallel channels, width $d = 1.5$, 4.0, 5.8, and 9.8 μm) were cast in PDMS (Poly(dimethylsiloxane)), and these replicas were used for the experiments.

The PDMS microstructures were plasma treated and irreversibly bound to glass cover slips which provides a tight seal. The microfluidic flow chamber is shown schematically in Fig. 1(b). The width of the microchannels covered one order of magnitude, whilst their length (2 cm) guaranteed translational invariance in the direction of the channels. The fact that we used many parallel channels enabled us to record images of several individual filaments at a time (Fig. 1(a)). To avoid adsorption of the actin filaments to the channel walls, the channel surfaces were coated with BSA (bovine serum albumin, 1 mg/ml) prior to filling the chamber with the dilute F-actin solution. We found that the filaments were fluctuating inside the channels without sticking for at least 24 h. Only data obtained from chambers with

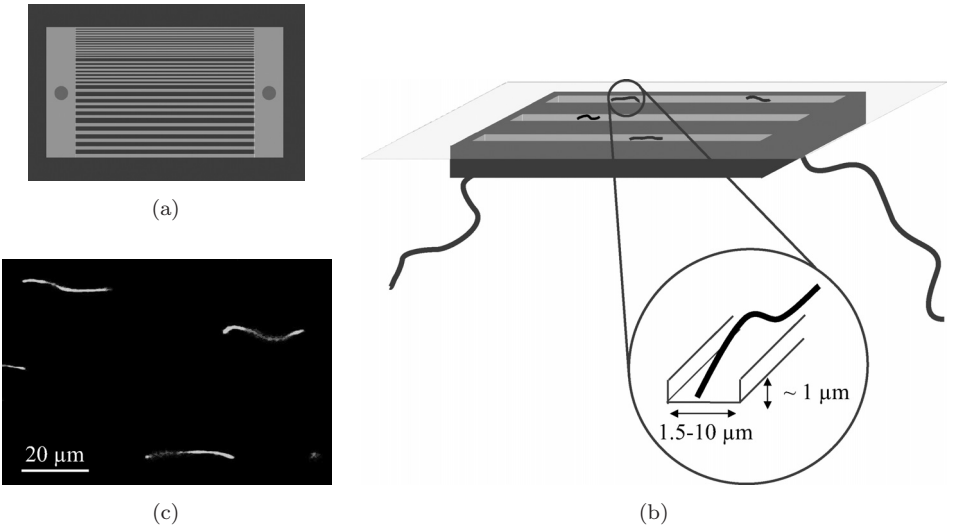

Fig. 1. (a) Schematic representation (top view) of the microfluidic channels. (b) Schematic representation of the flow chamber. (c) Fluorescence micrograph of multiple single actin filaments in microchannels.

negligible flow rates which had no influence on the dynamics of the filaments were analyzed.

We observed the contour fluctuations of the biopolymers with an Olympus BX61 fluorescence microscope equipped with a 75 W Xenon lamp and a 100x Plan Apochromat oil immersion objective. Movies were recorded using a PCO SensiCamQE CCD camera (exposure time 100 ms, 10 frames per second, see Fig. 1(c)). An actin concentration of 70 nM was chosen to secure investigations of individual actin filaments avoiding interactions between filaments. We observed F-actin in a quasi-2D system[21] since the channels had a depth of merely $\sim 1\,\mu$m and the contour line of each filament was projected into the focal plane of the microscope.

On length scales where molecular details are irrelevant, semiflexible polymers are best described by the continuum worm-like chain (WLC) model.[22,23] In the WLC model filament fluctuations are governed by the bending energy

$$\mathcal{H}_{\mathrm{WLC}} = \int_0^L ds \frac{\kappa}{2} \left[\partial_s \mathbf{t}(s)\right]^2 , \tag{1}$$

where κ is the bending rigidity of the filament, $\mathbf{t}$ is the unit tangent vector, and s is the arc length of the filament's contour. In the limit of a large contour length L the tangent correlation function of a WLC confined to a two-dimensional plane is exponentially decaying according to[22]

$$\langle \mathbf{t}(s) \cdot \mathbf{t}(s+l) \rangle = \exp\left(-l/2L_P\right) , \tag{2}$$

where the persistence length $L_P \equiv \kappa/k_B T$ is defined by the ratio of bending rigidity and thermal energy. The factor 2 in the denominator of the exponent in Eq. (2) is a consequence of the confinement to two dimensions.[4,5]

Using image analysis techniques, which are described in more detail below, for each microscopy image a set of tangent vectors $\mathbf{t}(s)$ is reconstructed from which the tangent correlation function $\langle \mathbf{t}(s) \cdot \mathbf{t}(s+l) \rangle$ is obtained by performing an average in time over all images of a movie. We also perform a spatial average over all points s within the same image (denoted by a bar) to obtain the quantity

$$\langle \cos\theta(l) \rangle \equiv \langle \overline{\mathbf{t}(s) \cdot \mathbf{t}(s+l)} \rangle . \tag{3}$$

To further improve the statistics of our results, we also average the data of several filaments where the same experimental parameters have been used.

In Fig. 2, semi-logarithmic plots of the experimental results for the tangent correlation functions for fluctuating filaments in microchannels of different widths are shown.[18] A minimum length of $L = 30\,\mu$m was chosen for this analysis to assure that the contour length of the filaments was large compared to the channel width d. For comparison, the dotted line shows the tangent correlation function for unconfined filaments (Eq. (2)). For sufficiently long observation times we measured

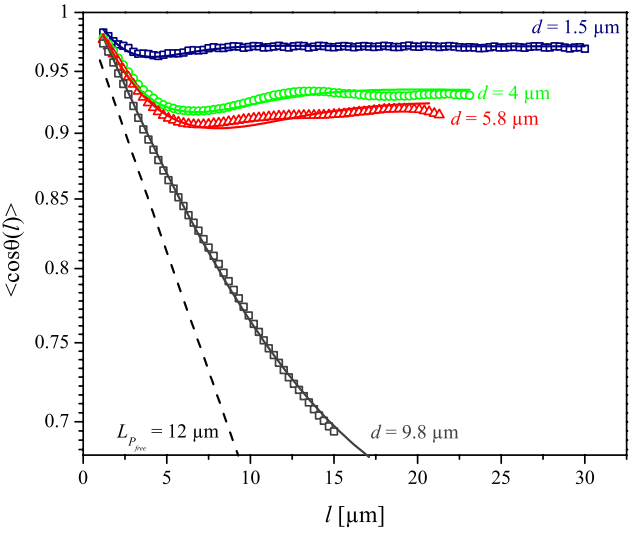

Fig. 2. Averaged tangent correlation functions of actin filaments confined in channels of different widths. Open symbols: experimental data; solid lines: fit curves using (5) in combination with the modified correlation function (13); dashed line: ideal tangent correlation function for free filaments.

the persistence length $L_P = 12\,\mu$m for unconfined filaments.[a] Clearly, filaments confined in $9.8\,\mu$m channels ($L \sim 3d$) are not very strongly influenced by the channel geometry; they show almost the same behavior as free filaments. For narrow channels ($d \leq 5.8\,\mu$m), however, a strong influence of the restraining channel walls is observed. The overall correlation increases with decreasing channel width, and the tangent correlation function develops a characteristic shape. This shape includes a local minimum, followed by a small oscillation about a saturation level: for large arc length separations l, the correlation function reaches a constant asymptotic value, instead of dropping to zero as for unconfined filaments. This asymptotic value increases with decreasing channel width, whereas the position of the minimum $l_{\min}$ decreases with decreasing channel width. These unique characteristics reflect that collisions with the confining channel walls lead to polymer turns and, thus, a re-correlation of tangent vectors at larger distances. The tangential orientations of two polymer segments which are far apart remain well correlated in contrast to the tangential vectors of a free polymer which decorrelate exponentially according to Eq. (2). The long-range correlation is not caused by a direct coupling of the segments, as in the case of a stiffer polymer with a larger persistence length, but by a coupling of all segments to the external confining potential which serves as a μm-scale track for the polymer.

[a]The values for the persistence lengths of free filaments are slightly smaller than the values obtained in Ref. 18 because of a longer observation time, which is now chosen sufficiently long that the measured values for the persistence length saturate.

3. Theory and Simulation of Tangent Correlations in Confinement

To understand and quantify the characteristic shape of the tangent correlation function in a more systematic way, we add a second term accounting for the confining channel geometry to the WLC-model (1). We approximate this term by a parabolic potential $Kz^2(s)/2$, where $z(s)$ is the displacement of the polymer perpendicular to the direction of the channels (with $z = 0$ corresponding to the center of the channel), and K is a constant value determining the strength of the potential. K has to be determined such that the effect from the confining channels is well described. This approach has been originally introduced by Helfrich in order to describe steric interactions of two-dimensional fluid membranes[24] and tubular vesicles.[25] As the actual interaction between polymer and channel walls is purely steric, we expect a temperature-dependent K, which increases with temperature T.

Including the parabolic potential we write the total energy in terms of the displacements $z(s)$ of the polymer perpendicular to the channel,

$$\mathcal{H} = \int_0^L ds \left[\frac{\kappa}{2} \left(\partial_s^2 z \right)^2 + \frac{K}{2} z^2(s) \right], \tag{4}$$

where we neglect higher order terms in $z(s)$. This approximation becomes exact in the limit of a weakly bent polymer or small displacement gradients $\langle (\partial_s z)^2 \rangle \ll 1$. Using the Hamiltonian (4), the tangent correlation function can be analytically calculated in the limit of large L:[26]

$$\begin{aligned} \langle \cos\theta(l) \rangle &\simeq 1 - \frac{1}{2} \langle (\partial_s z(s) - \partial_s z(s+l))^2 \rangle \\ &= 1 - \int_{-\infty}^{\infty} \frac{dq}{2\pi} q^2 G(q) (1 - \cos(ql)) \qquad (5) \\ &= 1 - \frac{\lambda}{2\sqrt{2} L_P} \left(\cos\left(\frac{\pi}{4}\right) - \cos\left(\frac{\pi}{4} + \frac{l}{\lambda}\right) \exp\left(\frac{-l}{\lambda}\right) \right), \qquad (6) \end{aligned}$$

where the correlation function of Fourier modes is given by

$$G(q) = \frac{k_B T}{\kappa q^4 + K}. \tag{7}$$

In addition to the persistence length L_P this result contains a second parameter, the *deflection length*

$$\lambda \equiv (4\kappa/K)^{1/4}, \tag{8}$$

which characterizes the competition of bending energy and confining energy in the parabolic potential. Eq. (6) shows that the deflection length is the correlation length of the confined polymer. For $l \gg \lambda$ tangent correlations reach the constant asymptotic value

$$\langle \cos\theta(l) \rangle = 1 - \langle (\partial_s z(s))^2 \rangle = 1 - \frac{\lambda}{4 L_P}, \tag{9}$$

which corresponds to uncorrelated fluctuations of free polymer segments of length λ. This shows that the approximation of small displacement gradients

$\langle(\partial_s z(s))^2\rangle \sim \lambda/L_P$ is valid for all l if $\lambda \ll L_P$ or for $l \ll L_P$ if $\lambda > L_P$. Therefore, in the limit of a small confining potential strength $K < k_B T/L_P^3$ corresponding to a large deflection length $\lambda > L_P$, the result (6) agrees only up to linear order in l/L_P with the exact result (2) for an unconfined semiflexible polymer.

The qualitative picture that emerges is as follows: at distances $l \sim \lambda$ collisions with the channel walls start to occur which lead to turns in the polymer contour. The onset of such polymer turns gives rise to a re-correlation of the tangent vectors and the characteristic minimum in the correlation function at $l_{\min} = 2\lambda/\pi$. On length scales $l < \lambda$ below this minimum, polymer segments are approximately free and the correlation function resembles the exponentially decaying free correlation function in this regime. On length scales $l > \lambda$ the polymer can be viewed as an ensemble of roughly uncorrelated segments of length λ leading to the constant asymptotic value (9).

We expect the same qualitative behavior of tangent correlations for any confining potential. The details of the particular confining potential only enter the numerical value for the deflection length λ. In particular, we expect the confining channels of width d to exhibit a similar behavior of tangent correlations as in (6) if λ is chosen such that the mean-square displacement $\langle z(s)^2\rangle \sim \lambda^3/L_P$ in the parabolic confining potential matches the expected mean-square displacement $\langle z(s)^2\rangle \sim d^2$ in the confining channel. This leads to[25, 27]

$$\lambda = a\, L_P^{1/3} d^{2/3} \tag{10}$$

(or a temperature-dependent $K = 4a^{-4} k_B T L_P^{-1/3} d^{-8/3}$), where a is a geometry-dependent numerical prefactor. It is not possible to justify the approximation of hard channel walls by a parabolic potential based on a systematic analytical treatment and to calculate the numerical prefactor a analytically. Therefore, we performed Monte Carlo simulations of fluctuating filaments in order to show that the tangent correlations in a confining channel of width d are indeed well described by Eq. (6), provided the expression (10) is used for the deflection length λ, and in order to determine the numerical prefactor a.

The Monte Carlo simulations were performed for the experimental geometry of rectangular channels with height $1.4\,\mu$m and widths $d = 1.5$, 2.5, 5.0, 7.5, and $10.0\,\mu$m and for filaments with persistence lengths $L_P = 10.0$, 15.0, and $20.0\,\mu$m. Details of the Monte Carlo simulations will be published elsewhere,[28] the main results for the tangent correlations are summarized in Fig. 3(a). In the Monte Carlo simulation we projected tangent vectors into two dimensions as in the experiment where the contour is projected into the focal plane and measured the spatially averaged tangent correlation function (3) for long filaments of $L = 100\,\mu$m. In combination with the relation (10) for λ, the result (6) can be used to collapse the rescaled tangent correlation data onto a single master curve using the relation

$$(1 - \langle\cos\theta(l)\rangle)\, d^{-2/3} L_P^{2/3} \simeq \mathcal{C}_a(l d^{-2/3} L_P^{-1/3}) \tag{11}$$

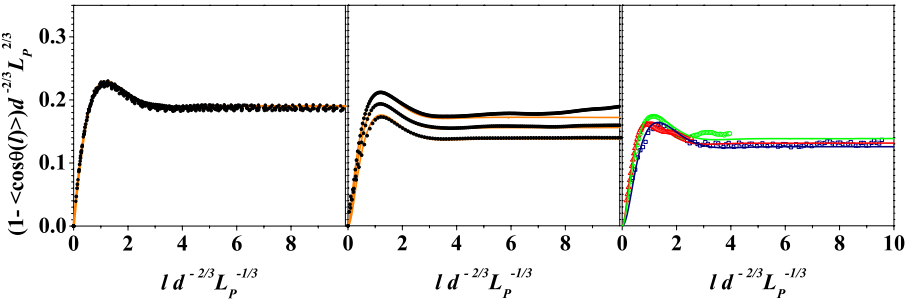

Fig. 3. Rescaled tangent correlation function $(1 - \langle\cos\theta(l)\rangle)\, d^{-2/3} L_P^{2/3}$ as a function of rescaled arc length separation $l d^{-2/3} L_P^{-1/3}$. (a) Monte Carlo data for an ideally thin and long filament ($L = 100\,\mu$m), channel widths $d = 1.5$, 2.5, 5.0, 7.5 and 10.0 μm, and persistence lengths $L_P =$ 10.0, 15.0, and 20.0 μm. The data collapse onto a single master curve (orange solid line) given by the shape function (12). (b) Monte Carlo data for a long filament ($L = 100\,\mu$m) with a simulated image radius of $R_{f,\mathrm{MC}} = 0.3\,\mu$m, channel widths $d = 1.5$, 2.5, and 5.0 μm, and a persistence length $L_P = 15.0\,\mu$m. The data are well described by the modified approximation formula (13) in combination with (5) (orange solid lines). (c) The same experimental data and fit curves as in Fig. 2 in rescaled form.

with a shape function

$$\mathcal{C}_a(x) \equiv \frac{a}{2\sqrt{2}}[\cos(\pi/4) - \cos(\pi/4 + x/a)e^{-x/a}], \tag{12}$$

which only depends on the geometry-dependent numerical prefactor a. In Fig. 3(a) it is demonstrated that Monte Carlo data for channels of different width d can indeed be collapsed onto a shape function of the form (12) with $a_{\mathrm{MC}} = 0.76$. This justifies the approximation of channel confinement by a parabolic confining potential and determines the geometry-dependent prefactor a in the scaling relation (10). The result (6) can therefore be used as the basis for the data analysis of tangent correlations within its range of validity, which is essentially given by the condition $\lambda \ll L_P$ as shown above. For confinement by channels of width d, this condition is equivalent to $d \ll L_p$ because of the scaling law (10). This shows that the polymer starts to perform turns within the confining channel if this condition is violated, and we obtain a crossover to the scaling behavior of a confined *flexible* polymer with a Kuhn segment length $2L_P$. Aspects of the modified scaling behaviour in the regime $d > L_p$ have been discussed in Ref. 15 for DNA.

4. Experimental Results and Data Analysis

The analysis of tangent correlations using the analytic approximation formula (6) is further complicated, however, by image analysis effects. In particular, filament images have a nonzero radius because of the intensity profile of fluorescent labels. The microscopy images were binarized and skeletonized to a one-pixel-line using commercial image processing software (Image-Pro Plus, AnalySIS, MATLAB).

To determine the tangent correlation, a cubic spline fit was applied to the one-pixel-line. An arc length reparametrization of the smoothed line was obtained by dividing it into tangent vectors of equal length. The correlation function of these tangent vectors as a function of the arc length separation l is calculated from their scalar products, see Eq. (3). The microscopy and image processing procedures we use slightly broaden the contour, due to restrictive optical resolution and thermal fluctuations during the exposure time of 100 ms. The effect leads to a superposition of slightly different conformations of the filament in one and the same fluorescence micrograph. The full width at half maximum (FWHM) of a filament, or effective width, in an original gray scale micrograph is ~ 0.3–$0.5\,\mu$m. After applying the appropriate threshold criterion to binarize the images, the filament's effective width is $\sim 1\,\mu$m. Since the actual diameter of F-actin is merely 8 nm, this implies that some small wavelength fluctuations cannot be visualized or analyzed. We account for this fact by introducing a correcting term in the theoretical description of the system. The local averaging of data over arc length distances similar to the filament image radius R_f can be taken into account by convoluting the correlation function of Fourier modes (7) with a Gaussian of width $\sim R_f$, which leads to

$$G_R(q) = \exp(-q^2 R_f^2)\frac{k_B T}{\kappa q^4 + K}. \tag{13}$$

For the analysis of experimental data we use $R_f = 0.5\,\mu$m, the radius of the filament image observed in the experiment. Fits of experimental data with the modified correlation function are performed using (13) in Eq. (5) and numerically evaluating the integral over wave vectors q.

In order to validate this method, we performed Monte Carlo simulations which (i) mimic the experimental data acquisition and (ii) use the same image analysis procedure to extract the final polymer contour. To mimic the experimental data acquisition, we introduce a pixel grid with the same pixel size as in the experiment and generate "microscopy images" in the simulation by illuminating each pixel that is touched by the polymer contour within a filament radius $R_{f,\mathrm{MC}}$ and over a certain exposure time.[28] Using this simulation procedure with a radius $R_{f,\mathrm{MC}} = 0.3\,\mu$m and a short illumination time we obtained the Monte Carlo data shown in Fig. 3(b) for the tangent correlation function, rescaled according to (11). The simulations were performed for a long filament ($L = 100\,\mu$m) with persistence length $L_P = 15.0\,\mu$m in channels of width $d = 1.5$, 2.5, and $5.0\,\mu$m, similar to the experimental situation. The orange solid lines in Fig. 3b show fits to this data using the modified correlation function with $R_f = 0.34, 0.30$, and $0.24\,\mu$m for $d = 1.5$, 2.5, and $5.0\,\mu$m, respectively, and our above result $a_{\mathrm{MC}} = 0.76$ for the numerical prefactor that characterizes the shape function (12). The quality of the fits demonstrates that the modified correlation function (13) allows for a quantitative description of image analysis effects. Furthermore, it shows that the parameter R_f in the modified correlation function corresponds, indeed, to the radius $R_{f,\mathrm{MC}}$ of the actual filament image. The plot of the rescaled data also shows that the data no longer collapses onto a single

master curve, because the additional small length scale $R_{f,\mathrm{MC}}$ becomes relevant. This leads to a splitting of the rescaled curves compared to the data shown in Fig. 3(a) for an ideally thin filament. Also the maximum of the rescaled curves in Fig. 3(b) is reduced. Both results can be qualitatively understood by observing that the nonzero radius R_f of the filament effectively reduces the channel width and, thus, enhances the tangent correlations.

The quality of the fits for the simulation results justifies the use of the modified correlation function for performing fits of the experimental data using a filament image radius $R_f = 0.5\,\mu$m as observed in the experiment. Using the modified tangent correlation function, we can obtain the persistence length L_P and the deflection length λ as independent fit parameters from the data. This improves the analysis presented in Ref. 18, where the persistence length L_P has been fixed to the value measured for a free polymer, and the deflection length λ was the only fit parameter. In discussing the data, we exclude the first few pixels ($\lesssim 2R_f = 1\,\mu$m) because this data is beyond the limits of the optical resolution.[3]

The solid lines in Fig. 2 show the results of this fitting procedure for different channel widths with good agreement. Figure 4 shows our results for the two independent fit parameters, the persistence length L_P and the deflection length λ. The numerical values for L_P scatter more, the wider the channel is. This is because a smaller channel leads to a smaller conformational space for the actin fluctuation and thus an improved statistics. The open symbols denote results for analysis of the tangent correlation functions of individual filaments while the closed symbols result from analysis of the averaged data including several individual filaments. All values lie in the same range and the mean value (dotted line) is $L_P = 13.1\,\mu$m, which agrees well with the value which we obtained for freely fluctuating experiments ($L_P = 12\,\mu$m). Figure 4(b) shows the results for λ for different channel widths. The dashed line marks the scaling law $\lambda \propto d^{2/3}$, see Eq. (10), which is confirmed by our

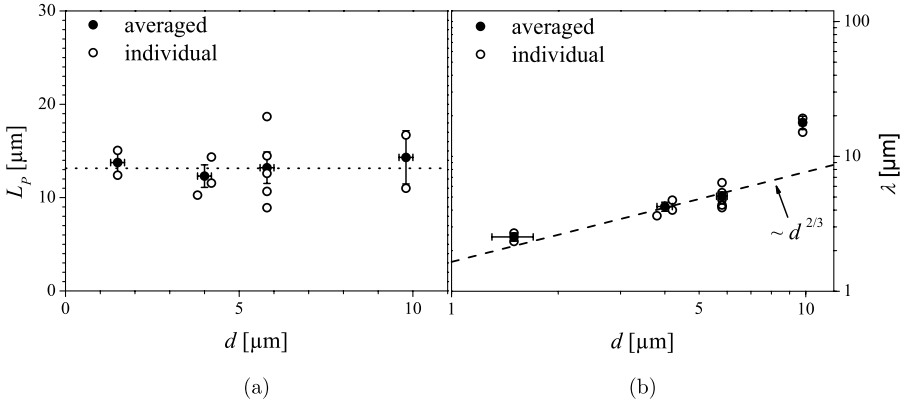

Fig. 4. (a) Persistence length L_P plotted against the channel width d. Dotted line: mean value 13.1 μm. (b) Deflection length λ plotted against the channel width d. Dashed line: scaling law.

experimental results. The results for λ obtained from experiments with $d = 9.8\,\mu$m show deviations from the predicted curve because the range of validity of Eq. (6) based on the assumption of a weakly bent polymer is limited to the regime $\lambda < L_p$ as shown in Sec. 3. This condition becomes violated for the measured values of $\lambda > 10\,\mu$m. The Monte Carlo simulations also indicate that Eq. (6) can no longer be applied in this regime.

To further investigate the validity of the scaling law (10) and compare experimental and simulation results, we present the data and the fits to the data of Fig. 2 in the same rescaled form as the simulation data in Fig. 3(c). The experimental data show a very similar behavior as compared to the simulation data for nonzero optical filament radius: the rescaled curves split in a similar way from a single master curve and the maximum of the rescaled curves is comparable. This suggests that the nonzero radius of the filament image is indeed the main cause of deviations from the behavior of ideal filaments, as described by Eq. (6). The fits give values $a = 0.65$–0.80 for the numerical prefactor that characterizes the shape function (12). These values agree well with our result $a_{\mathrm{MC}} = 0.76$ from Monte Carlo simulations, which demonstrates the validity of the scaling behavior (10). It is also evident that this scaling behavior can only be recovered if the modified analytical approximation formula (13) is used for the data analysis.

5. Conclusions

In summary, we were able to observe and quantitatively analyze thermal fluctuations of single semiflexible actin filaments in microchannels using fluorescence microscopy. We observed a strong dependence of the tangent correlation function of the fluctuating filaments on the channel geometry. The enhancement of the tangent correlation function and their unique characteristics can be analyzed using the analytical result (6) for the tangent correlation function. This result has been obtained using a confining parabolic potential in order to approximate the effects of confining microchannels and has been confirmed by additional Monte Carlo simulations of filaments confined to rectangular channels. We showed that deviations of experimental tangent correlation data from this analytical result are caused by image analysis effects, in particular, by the increased width of the filament image in fluorescence microscopy. To take this effect into account we provided the modified analytical approximation formula (13), which we validated by simulation of the imaging process. Including these corrections, both experimental and Monte Carlo data for rescaled tangent correlations can be described by the same shape function (12), which is characterized by a single numerical prefactor $a \simeq 0.76$, demonstrating the validity of the scaling law (10). A better understanding and further investigations of the interplay of an individual filament and its surrounding is not only crucial for understanding the mechanical properties of cellar processes, but also for the behavior of dilute polymer solutions in microfluidic applications.

Acknowledgments

We thank Stephan Herminghaus, Erwin Frey, Klaus Mecke, Cyrus R. Safinya, Myung C. Choi, Youli Li, and Reinhard Lipowsky for helpful discussions. This project was supported by the DFG in the framework of the Emmy Noether Programme (PF 375/2).

References

1. A. Alberts, D. Bray, J. Lewis, M. Raff, K. Roberts and P. Walter, *Molecular Biology of the Cell*, 4th edn. (Garland, New York, 2002).
2. L. Le Goff, O. Hallatschek, E. Frey and F. Amblard, *Phys. Rev. Lett.* **89**, 258101 (2002).
3. A. Ott, M. Magnasco, A. Simon and A. Libchaber, *Phys. Rev. E* **48**, R1642 (1993).
4. F. Gittes, B. Mickey, J. Nettelton and J. Howard, *J. Cell Biol.* **120**, 923 (1993).
5. H. Isambert, P. Venier, A. C. Maggs, A. Fattoum, R. Kassab, D. Pantaloni and M.-F. Carlier, *J. Biol. Chem.* **270**, 11437 (1995).
6. J. Käs, H. Strey, J. X. Tang, D. Finger, R. Ezzell, E. Sackmann and P.-A. Jamney, *Biophys. J.* **70**, 609 (1996).
7. T. Yanagida, M. Nakase, K. Nishiyama and F. Oosawa, *Nature* **307**, 58 (1984).
8. D. Riveline, C. H. Wiggins, R. E. Goldstein and A. Ott, *Phys. Rev. E* **56**(2), R1330 (1997).
9. J. Howard, *Mechanics of Motor Proteins and the Cytoskeleton* (Sinauer, Sunderland, 2001).
10. D. Boal, *Mechanics of the Cell* (Cambridge University Press, 2002).
11. J. Käs, H. Strey, M. Bärmann and E. Sackmann, *Europhys. Lett.* **21**, 865 (1993).
12. A. R. Bausch and K. Kroy, *Nature Physics* **2**, 231 (2006).
13. T. Pfohl, F. Mugele, R. Seemann and S. Herminghaus, *Chem. Phys. Chem.* **4**, 1291 (2003).
14. I. Y. Wong, M. L. Gardel, D. R. Reichman, E. R. Weeks, M. T. Valentine, A. R. Bausch and D. A. Weitz, *Phys. Rev. Lett.* **92**, 178101 (2004).
15. J. O. Tegenfeldt, C. Prinz, H. Cao, S. Chou, W. W. Reisner, R. Riehn, Y. M. Wang, E. C. Cox, J. C. Sturm, P. Silberzan and R. H. Austin, *P. Natl. Acad. Sci. USA* **101**(30), 10979 (2004).
16. J. Clemmens, H. Hess, J. Howard and V. Vogel, *Langmuir* **19**(5), 1738 (2003).
17. R. Bunk, J. Klinth, L. Montelius, I. A. Nicholls, P. Omling, S. Tågerud and A. Månsson, *Biochem. Bioph. Res. Co.* **301**, 783 (2003).
18. S. Köster, D. Steinhauser and T. Pfohl, *J. Phys.: Cond. Mat.* **17**, S4091 (2005).
19. Y. Xia and G. Whitesides, *Angew. Chem. Int. Ed.* **37**, 550 (1998).
20. E. Delamarche, A. Bernard, H. Schmid and H. Biebuyck, *Science* **276**, 779 (1997).
21. J. Hendricks, T. Kawakatsu, K. Kawasaki and W. Zimmermann, *Phys. Rev. E.* **51**, 2658 (1995).
22. L. D. Landau and E. M. Lifshitz, *Statistical Physics* (Pergamon Press, London, 1958).
23. O. Kratky and G. Porod, *Recl. Trav. Chim. Pay-B.* **68**, 1106 (1949).
24. W. Helfrich, *Z. Naturforsch. A* **33**, 305 (1978).
25. W. Helfrich and W. Harbich, *Chem. Scr.* **25**, 32 (1985).
26. L. Harnau and P. Reineker, *Phys. Rev. E* **60**, 4671 (1999).
27. T. Odijk, *Macromolecules* **16**, 1340 (1983).
28. S. Köster, J. Kierfeld and T. Pfohl, to be published.